Electronic Acknowledgement Receipt

EFS ID:	37670821
Application Number:	62931323
International Application Number:	
Confirmation Number:	9105
Title of Invention:	EUV Lithography System with Diffraction Optics
First Named Inventor/Applicant Name:	Kenneth Carlisle Johnson
Correspondence Address:	Kenneth Johnson - 2502 ROBERTSON RD - Santa Clara CA 95051 US - kjinnovation@earthlink.net
Filer:	Kenneth Johnson
Filer Authorized By:	
Attorney Docket Number:	
Receipt Date:	06-NOV-2019
Filing Date:	
Time Stamp:	12:46:03
Application Type:	Provisional

Payment information:

Submitted with Payment	yes
Payment Type	CARD
Payment was successfully received in RAM	$140

RAM confirmation Number	E2019A6C47592612
Deposit Account	
Authorized User	

The Director of the USPTO is hereby authorized to charge indicated fees and credit any overpayment as follows:

File Listing:

Document Number	Document Description	File Name	File Size(Bytes)/ Message Digest	Multi Part /.zip	Pages (if appl.)
1	Specification	2019_11_06_ProvisionalSpec.pdf	82219 567e93b766cb193e15386ed58141a137df5a6b81	no	11
Warnings:					
Information:					
2	Drawings-other than black and white line drawings	2019_11_06_ProvisionalDrawings.pdf	1275818 2739eb8fcf36fb9ca9f7b5e035206ec2809a286b	no	20
Warnings:					
Information:					
3	Fee Worksheet (SB06)	ProvisionalSB_.pdf	80306 fa43c4c182e080a46c2ec55f36aa9e5292c66b9c	no	3
Warnings:					
Information:					
4	Fee Worksheet (SB06)	fee-info.pdf	29361 43fe17c3e4764870ae0fe8c3317efe7b20612105	no	2
Warnings:					
Information:					
			Total Files Size (in bytes):	1467704	

This Acknowledgement Receipt evidences receipt on the noted date by the USPTO of the indicated documents, characterized by the applicant, and including page counts, where applicable. It serves as evidence of receipt similar to a Post Card, as described in MPEP 503.

New Applications Under 35 U.S.C. 111

If a new application is being filed and the application includes the necessary components for a filing date (see 37 CFR 1.53(b)-(d) and MPEP 506), a Filing Receipt (37 CFR 1.54) will be issued in due course and the date shown on this Acknowledgement Receipt will establish the filing date of the application.

National Stage of an International Application under 35 U.S.C. 371

If a timely submission to enter the national stage of an international application is compliant with the conditions of 35 U.S.C. 371 and other applicable requirements a Form PCT/DO/EO/903 indicating acceptance of the application as a national stage submission under 35 U.S.C. 371 will be issued in addition to the Filing Receipt, in due course.

New International Application Filed with the USPTO as a Receiving Office

If a new international application is being filed and the international application includes the necessary components for an international filing date (see PCT Article 11 and MPEP 1810), a Notification of the International Application Number and of the International Filing Date (Form PCT/RO/105) will be issued in due course, subject to prescriptions concerning national security, and the date shown on this Acknowledgement Receipt will establish the international filing date of the application.

EUV Lithography System with Diffraction Optics

Inventor: Kenneth C. Johnson, November 6, 2019

This disclosure replicates (with minor corrections) and supplements Provisional Application 62911467, filed on October 7, 2019. New material is added under the header "November 6, 2019 Addendum".

Abstract

A spot-scanning, maskless EUV lithography system using singlet zone-plate lenses for spot generation exhibits significant chromatic dispersion, but the dispersion can be neutralized by means of a diffractive, phase-Fresnel mirror in the projection optics. The same dispersion compensation method can be used in the context of EUV mask-projection lithography using a diffractive photomask, which can focus illumination onto sparse image patterns for high-dose, aberration-free printing.

Background

US Patent 9,097,983 (hereafter '983) discloses a scanned-spot-array, maskless lithography system in which diffractive microlenses focus EUV illumination onto an array of focus spots at the object plane of a projection system, which images the spot array onto a printing surface at reduced magnification. The spots are individually modulated by MEMS shutters at the focal plane as the printing surface is scanned across the spot-array image to synthesize a digital, high-resolution raster image. Recent improvements on the '983 disclosure are described in Ref's. 1 and 2.

The microlenses exhibit strong chromatic dispersion, which can be neutralized by using microlens doublets in an achromatic, Schupmann configuration as illustrated FIG. 10 in '983. The paired lenses are formed on opposite sides of a microchannel plate, which would be formed by bonding two half-plates at the focal plane with the MEMS shutters sandwiched between them.

The lenses are phase-Fresnel elements blazed for high efficiency in the first diffraction order. Phase-Fresnel lenses are needed in part to overcome the efficiency limitation of conventional zone-plate lenses, and also to minimize stray light in extraneous diffraction orders. Stray light from the first lens is not a problem because it can be spatially filtered at the focal plane. But the second lens would generate extraneous diffraction orders within the projection system's acceptance range, and the lens blazing would need to be accurately controlled to limit the energy in these orders. The technology for manufacturing these types of blazed EUV lenses has not yet been developed.

Achromatic lenses are needed because EUV lithography systems typically use laser-produced plasma (LPP) sources, which have a spectral bandwidth of approximately 3% after spectral filtering by the EUV mirrors (assuming four near-normal-incidence mirrors between the plasma and the writing surface). If the source were monochromatic then simpler singlet lenses could be used. The lenses could be conventional binary (two-level) zone plates such as those described in Ref. 3. A binary lens has only about half the efficiency of a phase-Fresnel lens, but with only one lens the efficiency would be comparable to a phase-Fresnel doublet. Binary lenses also exhibit a high degree of scattering into extraneous order, but these orders could be filtered out at the focal plane.

Summary of the Invention

Diffractive singlet microlenses can be used in a maskless EUV lithography system with a broadband EUV source by incorporating dispersion correction in the projection system. At least one projection mirror is formed as a blazed, phase-Fresnel diffractive element, which induces chromatic aberration to offset and nullify the lens chromatic aberration. (The lenses concomitantly neutralize the projection system's monochromatic aberrations.) In one embodiment, the projection system is a two-mirror, flat-field Schwarzschild projector in which the larger mirror is formed as a diffractive element.

The same dispersion-compensation mechanism can be used in the context of mask-projection lithography, in a configuration similar to the maskless system except that the microlens array is replaced by a diffractive ("holographic") photomask. The mask – like the microlens array – is displaced from the focal plane (i.e., the projection system's object plane). An advantage of this type of diffractive imaging is that the mask can concentrate illumination onto sparse image patterns to achieve much higher dose levels than are possible with conventional focal-plane masks. A diffractive mask can also nullify projection system aberrations.

Description of Specific Embodiments

FIG. 1 shows a cross-sectional optical schematic of a maskless EUV scanner similar to that described in '983 and Ref's. 1 and 2, but using singlet microlenses and with dispersion compensation incorporated in the projection system. An LPP plasma **101** generates EUV radiation, which is focused by an ellipsoidal collection mirror **102** to an intermediate focus IF, where it is spatially filtered by a small aperture. (The LPP power may be shared by other scanners **103**.) The IF-transmitted radiation is directed by two illumination mirrors, grazing-incidence element **104** and near-normal-incidence element **105**, onto microlens array **106**. The microlenses partition the radiation into approximately 2 million individual point-divergent beams, which are focused by two axially-symmetric Schwarzschild mirrors M1 and M2 onto an array of diffraction-limited focal spots on a writing surface **107**. The beams are individually modulated as the surface **107** is scanned across the spot array to synthesize a digital, high-

resolution raster image. (FIG. 1 appears identical to the prior art but in the present context the lenses are singlets and mirror M2 is diffractive.)

The M2 mirror, as described in Ref's. 1 and 2, has a diameter of 600 mm. The projection system has a numerical aperture (NA) of 0.55 and demagnification factor of 6.3×, and the image field diameter is 5 mm. The system's operating wavelength is 13.5 nm, and the LPP source is a an Adlyte system (Ref. 4), which can operate at a pulse rate of about 24 kHz or possibly as high as 50 kHz.

FIG. 2 schematically illustrates the scan process. The focal spot array **201** writes a raster line pattern as the writing surface **107** scans from left to right in the figure. For example, spot **202** writes line **203**. The scanning process is described in detail in Ref. 2.

FIG. 3 shows an enlarged cross section of the microlens array **106**, which is formed as a structured, topographic pattern layer **301** on a thin (e.g. 50-nm) Si substrate **302** supported by a microchannel plate **303**. Each microlens, such as element **304**, focuses illumination into a beam converging toward and through a focal point **305** on the projection system's object plane. Conical holes are formed in the plate to accommodate the beam paths. A MEMS shutter **306** modulates the beam at or near the focal point, in synchronization with the LPP pulse rate.

Microlens element **304** is illustrated in FIG. 4A in cross-section, and in FIG. 4B in plan view. (For clarity of illustration the depth dimensions are exaggerated and only 12 phase periods are shown.) Phase-Fresnel lenses would be preferred for high efficiency, but conventional binary zone-plate lenses (as illustrated) could be more easily manufactured. Each lens can comprise a pattern of concentric, annular rings formed by etching a thin (e.g. 85-nm) Mo film **301** on the Si substrate **302**. Practical fabrication details are discussed in Ref. 3.

The annular rings are illustrated as concentric circles in FIG. 4B, but the actual shapes would typically be elliptical and distorted to compensate for optical aberration (mainly astigmatism) in the projection system. Each lens generates an optical wavefront that emerges from the projection system as a spherical, point-convergent beam without aberration.

For specificity of illustration, the lens diameters can be approximately 15 microns. The lens numerical aperture is 0.087 (i.e., the projection system's NA, 0.55, divided by the demagnification ratio, 6.3), and the lens focal length (microchannel plate depth) is 86 microns. Each lens has about 24 phase periods, and the minimum period dimension is 150 nm. The microlens array fits within an object field of diameter 31.5 mm (i.e., the image field diameter, 5 mm, times 6.3), and can have the layout pattern described in Ref. 2. As illustrated in Fig. 20 of Ref. 2, the array is partitioned into four rectangular subarrays, each of width 6 mm ("A" dimension in Fig. 20 and Eq. 43 of Ref. 2). The array should maintain a flatness and height position within a tolerance range of approximately ±0.5 micron. If necessary, a honeycomb structural support can be formed on the microchannel back side (in the space between the diverging beams) to provide added rigidity.

The singlet lens system is simpler than the Schupmann doublet lenses described in '983 and Ref's. 1 and 2. It avoids the complication of a double-microchannel-plate assembly with MEMS

shutters and electronics sandwiched between the plates. The elimination of the extra lens element improves efficiency, and the problem of optical scatter from the second lens is also eliminated. The singlet lenses have twice as much optical power, and thus twice as many phase zones, as the doublet elements, but this would not pose a problem for manufacturing if binary zone plates are used. The lower efficiency of zone-plate lenses relative to phase-Fresnel lenses is offset by the efficiency gain from eliminating the second lens element.

A singlet lens is not corrected for chromatic dispersion, which causes longer wavelengths to be more strongly diffracted than shorter wavelengths. For a 3% source spectrum, the 86-micron focal length will be dispersed over a 2.6-micron focal range, resulting in a defocus phase error on the order of one-half wave. This level of phase decoherence would be significant for high-performance lithographic imaging.

The chromatic dispersion can be substantially reduced or eliminated by putting a blazed diffraction structure on at least one of the projection mirrors such as the M2 element in FIG. 1. The number of grating phase zones on the mirror would be approximately equal to the number of lens phase zones, e.g. 24 for the above-outlined design conditions. The minimum zone width for a mirror of diameter 600 mm would be approximately 6 mm.

The mirror grating could potentially be fabricated by forming the mirror substrate with step discontinuities at the zone boundaries. The step depths would be in the range of 7 to 10 nm, depending on the local incidence angle, and the structured substrate would be coated with a standard multilayer reflective coating, e.g. 50 or more Mo/Si bilayers with a bilayer thickness equal to the grating step depth. (Mo/Si mirrors are generally used for an operating wavelength of 13.5 nm.) FIG. 5A shows a schematic cross-sectional view of M2 with the grating structure, and FIG. 5B shows a plan view. One particular grating step **501** is illustrated in an expanded cross-sectional view in FIG. 6, which schematically illustrates the Mo/Si multilayer **601**. These types of "conformal multilayer" gratings are known in the prior art (although not for this application), e.g., see FIG. 5 in U.S. Patent 9,612,370.

However, diffractive mirrors with such wide zones (over 6 mm) could be formed more simply by depositing the Mo/Si bilayers on a standard, unpatterned substrate, and masking some of the layer depositions to form the blaze structure. FIG. 7 illustrates the M2 cross-section with this type of structure. The step **501** is formed by masking one of the bilayer depositions, e.g. by using a proximity mask **701** during the magnetron sputtering operation. The mirror could be formed by first depositing 50 or more standard Mo/Si bilayers on the substrate, and then depositing 24 more bilayers using a sequence of circular or annular masks on successive bilayers to define the steps.

Better optical performance with less optical scatter might be achieved by tapering the bilayer thicknesses near the mask edge to form a continuous surface **801** through the Mo/Si layers with no step discontinuities, FIG. 8. In this case the zone boundaries are not defined by surface steps; they are rather defined by some reference boundary in the multilayer such as the boundary interface between a lower Mo layer and an upper Si layer. The edge taper can be formed by rotating the mirror under a mask with a spiral or serrated edge during the deposition process. A

separate mask would be needed for each Mo and Si layer. Alternatively, a variable-size mask such as an iris diaphragm or conical-foil aperture mask could be used to continuously vary the mask diameter, avoiding the need for a mask change after every layer deposition.

In another variant process, the diffracting structure can be formed by first forming a standard Mo/Si multilayer on an unpatterned substrate, and then using a process such as ion beam figuring to selectively remove material, leaving a boundary surface that is tilted relative to the Mo/Si layers as illustrated in FIG. 8.

The above-described dispersion compensation method can also be applied to mask-projection lithography by replacing the microlens array with a transmission mask. (An alternative embodiment using a reflection mask will be described below.) The mask would be a free-standing, pellicle-type film (e.g. 50-nm Si, similar to element **302** in FIG. 3 but without the supporting microchannel plate **303**) on which a diffracting pattern is formed (similar to pattern layer **301** in FIG. 3). The mask pattern is not in the object plane; it is displaced some distance in front of or behind the image plane (e.g. 86 microns from the object plane, based on the above-outlined design parameters). The mask produces a diffraction pattern, which forms the image pattern on the writing surface in a manner analogous to “holographic lithography” (U.S. Patents 6,618,174 and 9,940,694, and Ref. 5).

One advantage of this type of diffractive imaging is that it would greatly improve the exposure dose for sparse image patterns. For example, in printing a contact hole pattern a diffractive mask could focus most of the available illumination energy onto a focal point array defining the contact holes.

Another advantage of diffractive imaging is that the mask can correct aberrations in the projection system in much the same way that the microlenses in a maskless, spot-scanning system do. This assumes that the mask is used in a static imaging mode (i.e., step-and-repeat, not scanning).

Diffractive imaging would be relatively insensitive to isolated mask defects because the defects are not in focus at the printing surface. Diffractive imaging might also provide unique capabilities for resolution enhancement, e.g. via selective spatial frequency filtering.

A diffractive mask would generally need to control both the phase and amplitude of the transmitted beam. But the design has many degrees of freedom because the mask only needs to control the phase and amplitude of spatial frequencies within the projection system’s acceptance range. For example, rather than using an absorber material to control the beam intensity, the image-plane intensity level could be controlled by diffractively scattering radiation outside of the acceptance range via phase modulation.

Diffractive imaging requires a high-brightness, compact EUV source because the source size limits resolution. The geometric image of the source on the writing surface (after spatial filtering at the IF, FIG. 1) should be significantly smaller than the diffraction limit. (In Ref. 2, the IF filter’s geometric image has a diameter of 7.8 nm, resulting in a 5% increase in the diffraction point-spread function’s width relative to an ideal point source.)

Diffractive imaging is also limited by chromatic dispersion, but this limitation is overcome by the compensating diffractive mirror in the projection optics as described above.

A transmission mask would need to be sufficiently thin to have good EUV transmission. If a single mask covering the entire object field (e.g., 31.5-mm diameter) would not be rigid enough to stay flat within a submicron sag tolerance, then the mask can be partitioned into several sub-apertures as illustrated in FIG. 9 in plan view. Within the object field **901**, four sub-aperture masks (e.g. mask **902**) of narrow width (e.g. less than 5 mm) have apodized transmittance characteristics represented by the shaded patterns (or are illuminated with apodized radiation fields). The masks form the image-plane exposure pattern **1001** illustrated in FIG. 10A. The dashed rectangles in FIG. 10A (e.g. rectangle **1002**) illustrate the nominal image field dimensions, although the apodized exposure area extends across these boundaries. After the image is exposed, the writing surface is stepped and a second mask is used to fill in the image field (FIG. 10B). The exposures overlap over their apodization zones. Multiple additional stepping and mask-change operations are performed (e.g., FIGS. 10C, 10D) to cover an extended image field. The image apodization enables field stitching without edge diffraction artifacts.

The sub-aperture partitioning is inefficient because it uses only a fraction of the available illumination energy. This limitation can be overcome by using a reflection mask, which can have a thick structural backing similar to conventional EUV reflection masks, and therefore need not be partitioned into narrow sub-apertures. Near-normal-incidence illumination can be projected onto the mask as illustrated in FIG. 11. This configuration is similar to FIG. 1, except that mirror **105** directs the radiation onto mirror **1101** in the projection system's obscuration zone, and mirror **1101** reflects the radiation onto reflection mask **1102**. (Mirror **1101** can be supported by spider vanes or tension wires crossing the optical path.)

The mask illumination is not exactly normally-incident, except at the center, because the projection system is not telecentric in the object space. But the incidence angle at the edge of the object field is only 0.8º in the FIG. 11 configuration. The illumination could be made normally-incident over the full mask by designing the optics for a curved object surface and using a correspondingly curved mask surface. The curvature sag would be 0.1 mm across the 31.5-mm object field.

FIG. 12 illustrates a possible layout for the reflection-mask **1102** in plan view. A cross-shaped mask aperture is used to achieve a high fill factor within the circular object field **901**. The mask has an apodized reflection characteristic (or the illumination is apodized) as indicated by the shaded area in FIG. 12, resulting in the apodized exposure image **1301** illustrated in FIG. 13A. The nominal image field boundary is indicated by dashed polygon **1302**, although the apodized exposure slightly overfills this boundary. The writing surface is stepped, and the mask is changed, to expose an adjacent image field (FIG. 13B), and subsequent stepping and mask-change operations are used to cover an extended image field (e.g., FIG. 13C).

An advantage of this system over conventional EUV lithography is that the mask operates at normal incidence (or near-normal incidence), so mask shadowing and 3-D effects would have

comparatively impact. Also, with the diffractive imaging technique the mask design might have sufficient degrees of freedom to nullify 3-D effects.

Cited Patents

1. US Patent 9,097,983
2. U.S. Patent 9,612,370
3. U.S. Patent 6,618,174
4. U.S. Patent 9,940,694

References

1. K. Johnson, “Maskless EUV Lithography”, presented at the 2019 EUVL Workshop [https://www.euvlitho.com/2019/P22.pdf]
2. Kenneth C. Johnson, “Maskless EUV lithography, an alternative to e-beam,” *J. Micro/Nanolith. MEMS MOEMS* 18(4), 043501 (2019) [https://doi.org/10.1117/1.JMM.18.4.043501]
3. F. H. Salmassi, W. Chao, E. M. Gullikson, J. Meyer-Ilse, and P. P. Naulleau, “Fabrication and performance of transmission engineered molybdenum-rich phase structures in the EUV regime”, in *International Conference on Extreme Ultraviolet Lithography* **10450**, p. 104501B. International Society for Optics and Photonics (2017) [https://doi.org/10.1117/12.2281487]
4. F. Abhari, “Status of Adlyte’s light source for inspection tools”, presented at the 2019 EUVL Workshop [https://www.euvlitho.com/2019/P42.pdf]
5. “Sub-Wavelength Holographic Lithography”, Nanotech SWHL GmbH [https://nanotech-swhl.com/index.html]

<u>November 6, 2019 Addendum</u>

The M2 grating structure illustrated in FIGS. 5A, 6, 7, and 8 was described as a "blazed" grating. The "conformal multilayer" grating in FIG. 6 is a type of blazed grating, but the structures illustrated in FIGS. 7 and 8 are more accurately described as "Bragg diffraction gratings". Although the FIG. 7 structure has a sawtooth-type surface geometry similar to blaze gratings, the surface topography is not the primary diffraction mechanism and can actually degrade performance. The primary diffraction mechanism is the tilt of the bilayers relative to the surface, e.g. as illustrated in FIG. 8.

Prior-art holographic lithography systems are described in previously-cited U.S. Patents 6,618,174 and 9,940,694, and in Ref. 5. Other relevant prior-art includes US Patent 7,499,149 and Ref. 6, listed at the end of this disclosure.

FIG. 14 shows a portion of the FIG. 1 optical system, which is adapted for holographic lithography with a transmission mask **1401**. Enlarged views are shown in FIGS. 15A and 15B. Mirror **104** is segmented to divide the reflected beam into four separate beams, which are directed by four mirrors **1501a**, **1501b**, **1501c** and **1501d** onto respective sub-aperture masks **902a**, **902b**, **902c**, and **902d** comprising mask **1401** (with **902a** corresponding to **902** in FIG. 9). The beam paths are shaded for clarity. The beam partitioning minimizes fill factor losses at the mask.

The mirrors **1501a** … **1501d** can be apodized to provide apodized illumination profiles on masks **902a** … **902d**. The mirror reflectance can be apodized, for example, with a gradient-thickness absorber layer on the mirror periphery, or with a half-tone grating pattern (either a phase or absorption grating) similar to that described in U.S. Patent 5,859,424.

FIGS. 16A, 16B, and 16C show schematic cross-sectional views of the transmission mask **1401** (FIG. 15B) in three alternative embodiments. In FIG. 16A the mask precedes the projection system's object plane **1601** in the optical path. A portion **1602** of the mask focuses illumination **1603** to an isolated point image **1604**, in much the same way that the microlenses in a maskless system do (FIG. 3). However, there is no focal-plane filtering of the image, so the mask would require a diffraction pattern having the form of a phase-Fresnel lens, which is accurately blazed to minimize scattered radiation.

A second portion **1605** of the mask is illustrated as comprising a diffraction grating, which creates a dense line/space pattern via interference between the grating's first and minus-first diffraction orders. This is basically a small-scale implementation of interference lithography (Ref. 7).

For a 13.5-nm operating wavelength the mask can comprise a thin (e.g. 50-nm) Si substrate **1606**, similar to an EUV pellicle, supporting a diffracting structure **1607** formed as a patterned, multilevel Mo layer. For some applications an absorber material (e.g. TaN) might be included in the structure, but the FIG. 16A structure does not use an absorber (except to the extent that Mo has some unavoidable absorption).

Contact hole arrays can be formed using two-level checkerboard phase patterns (Ref. 8) or a four-level, stepped spiral-phase pattern (see FIG. 20 in U.S. Patent 8,994,920). For EUV applications the quadrant phase shifts for a stepped, spiral-phase pattern would need to be modified to account for the Mo absorption. (With no absorption, the phase shifts are 0, 90º, 180º, and 270º; for Mo at wavelength 13.5 nm the estimated phase shifts are 0, 85.229º, 163.367º, 274.771º.)

FIG. 16B is similar to FIG. 16A except that the mask **1401** follows the object plane **1601** in the optical path.

A more conventional focal-plane mask **1401** located at object plane **1601** could be used, as illustrated in FIG. 16C. The image features are defined by an attenuator layer **1608**. But this would forfeit the advantages of holographic masks including include high optical efficiency, aberration compensation, and minimal defect sensitivity.

The beam paths through the projection system in FIGS. 1 and 14 have a shadow region created by the M1 and M2 annular mirror obscuration, in which a blocking mask **1701** can be located as a zero-order stop as illustrated in FIG. 17. This simplifies the mask design because there is no need for zero-order extinction. For example, portions of the mask that are intended to produce a dark (zero-intensity) image can simply be unpatterned; there is no need for an absorber or diffractive extinction of the zero order. The system operates in darkfield imaging mode. If a bright field is needed (e.g. for flood exposure) then a blazed phase grating can be formed on the mask to direct radiation outside of the obscuration zone.

The blocking mask **1701** can be supported by either spider vanes, tension wires, or a pellicle crossing the optical path.

A flat reflection mask **1102** in FIG. 11 can be illuminated at normal incidence with a collimated illumination beam. (The mask substrate actually need not be curved for normal incidence, as stated in the October 7, 2019 disclosure.) For example, according to the design data in Ref. 2 the obscuration shadow region can accommodate a mirror **1101** of diameter up to 35.7 mm, larger than the object field diameter of 31.3 mm, so there is sufficient space to accommodate a collimated or slightly convergent illumination beam. FIG. 18 shows a portion of the FIG. 11 system with a flat mirror **1101** and collimated illumination beam. Mirror **1101** can be apodized to provide an apodized illumination profile on mask **1102**.

Mirror **1101** can operate as a zero-order stop, reflecting zero-order radiation from the mask back to the source. As with the blocking mask **1701** in FIGS. 14 and 15, the mirror **1101** can be supported by either spider vanes, tension wires, or a pellicle.

The reflection mask **1102**, illustrated with a cross-shape geometry in FIG. 12, can have any shape that can be periodically tiled. A hexagonal mask field **1102** (or mask illumination field), illustrated in FIG. 19, could be used to optimize optical efficiency. A hexagon has a fill factor of 82.7% within an enclosing circle, compared to 76.4% for a cross shape, and 63.7% for a square.

The preceding design examples for wavelength 13.5 nm, using Mo and Si, can be adapted for other wavelengths. For example, at wavelength 6.7 nm Mo could be replaced by La and Si can be replaced by B or B4C (Ref. 9).

The holographic lithography method described above is a step-and-repeat process, i.e., the mask and writing surface are substantially stationary during exposure. This is simpler than conventional lithography scanners, in which the alignment between the mask and wafer (writing surface) must be controlled to nanometer-scale accuracy while both are moving at a relative speed of 3.5 m/sec (Ref. 10).

With field stitching (e.g., as illustrated in FIGS. 10B, 10C, 10D, 13B and 13C), large writing fields of any size can be covered with relatively small masks. But throughput would be limited by the multiple mask and wafer load and alignment operations. To optimize the EUV source productivity, the source can be switched between different stepper modules, e.g. by means of movable, beam-diverting mirrors, to minimize source idle time during loading and alignment.

Field stitching requires accurate alignment of the mask and the writing surface. Prior-art alignment mechanisms such as imaging targets, diffraction gratings and Moiré patterns (typically using visible or infrared radiation) can be employed. Alternatively, a surface profilometry approach, similar to methods that have been proposed for EUV mask inspection and servo control for machining operations, could be adapted for mask/wafer alignment. (See U.S. Patent 10,025,079 and Ref's. 11 and 12.) The operational principle of this method is illustrated in FIGS. 20A and 20B. An alignment mark **2001** is formed in an optically reflective surface **2002** as a topographic feature such as a surface indentation (as illustrated), protrusion, or step discontinuity, or as any phase-modifying optical feature. An optical probe beam **2003** is focused onto the target, and the reflected beam is directed onto a position-sensing detector PSD, which detects variations in the reflection angle or in the far-field beam intensity pattern as the surface steps or scans across the beam. (Focusing optics and collection optics preceding the PSD are not shown in FIGS. 20A and 20B.) Multiple probe beams can be generated, e.g. via a microlens array, for simultaneous sensing of multiple alignment targets. The system can use off-axis (as illustrated) or on-axis illumination, and the detection light path can pass through the lithography stepper's projection optics (in "through-the-lens", or TTL, operational mode). This technique can provide very sensitive and accurate positional feedback using relatively small alignment targets.

TTL focus sensing can also be performed, e.g. by using an astigmatic confocal method (Ref. 13). FIG. 21 schematically illustrates an adaptation of the method for lithography. A small light source **2101** such as a laser diode or optical fiber illuminator directs a light beam **2102** through beam-forming optics (optional, not shown) and through a lithography projection system **2103**. The beam-forming optics and projection system in combination bring the beam to a focus **2104** on a reflective surface **2105**. The focus is astigmatic (either due to astigmatism inherent in the projection system, or from astigmatism added by the beam-forming optics), so after reflecting from the surface and propagating back through the projection optics the return beam will form a generally elliptical halo on the source plane **2106**, with the ellipticity varying in relation to the surface's focus height. FIGS. 22A, 22B, and 22C illustrate the reflection halo **2201** for three

slightly different focus positions. A quadrant detector **2202** in the source plane, comprising four detector elements, is sensitive to the ellipticity variation and provides a precise and accurate focus height measurement.

Additional Cited Patents

5. US Patent 7,499,149
6. U.S. Patent 5,859,424
7. U.S. Patent 8,994,920
8. U.S. Patent 10,025,079

Additional References

6. Deuter, V., et al. "Holographic masks for computational proximity lithography with EUV radiation." *International Conference on Extreme Ultraviolet Lithography 2018*. Vol. 10809. International Society for Optics and Photonics, 2018. [https://doi.org/10.1117/12.2502879]
7. Päivänranta, Birgit, et al. "Sub-10 nm patterning using EUV interference lithography." *Nanotechnology* 22.37 (2011): 375302. [http://dx.doi.org/10.1088/0957-4484/22/37/375302]
8. Naulleau, Patrick, et al. "Ultrahigh efficiency EUV contact-hole printing with chromeless phase shift mask." *Photomask Japan 2016: XXIII Symposium on Photomask and Next-Generation Lithography Mask Technology*. Vol. 9984. International Society for Optics and Photonics, 2016. [https://doi.org/10.1117/12.2243321]
9. Torsten Feigl et al., "Multilayer Optics for 1 nm to 13.5 nm: Can we reduce the litho wavelength further?", 2018 International Workshop on EUV and soft X-Ray Sources [https://www.euvlitho.com/2018/S18.pdf]
10. F. Bornebroek, "TWINSCAN scanner evolution enabling 5000 wafers per day," ASML Images, Fall Edition, 2008. [https://staticwww.asml.com/doclib/productandservices/images/2008/Fall/Articles/Images_Fall_Edit_2008%2014-15.pdf]
11. K. Johnson, "Application of EUV Diffraction Optics for Actinic Mask Inspection and Metrology", presented at the 2018 EUVL Workshop [https://www.euvlitho.com/2018/P36.pdf]
12. K. Johnson, "Accurate Tool Servo Control for Precision Diamond Turning", 2019. [http://vixra.org/pdf/1809.0447v2.pdf]
13. Cohen, Donald K., et al. "Automatic focus control: the astigmatic lens approach." *Applied optics* 23.4 (1984): 565-570. [https://doi.org/10.1364/AO.23.000565]

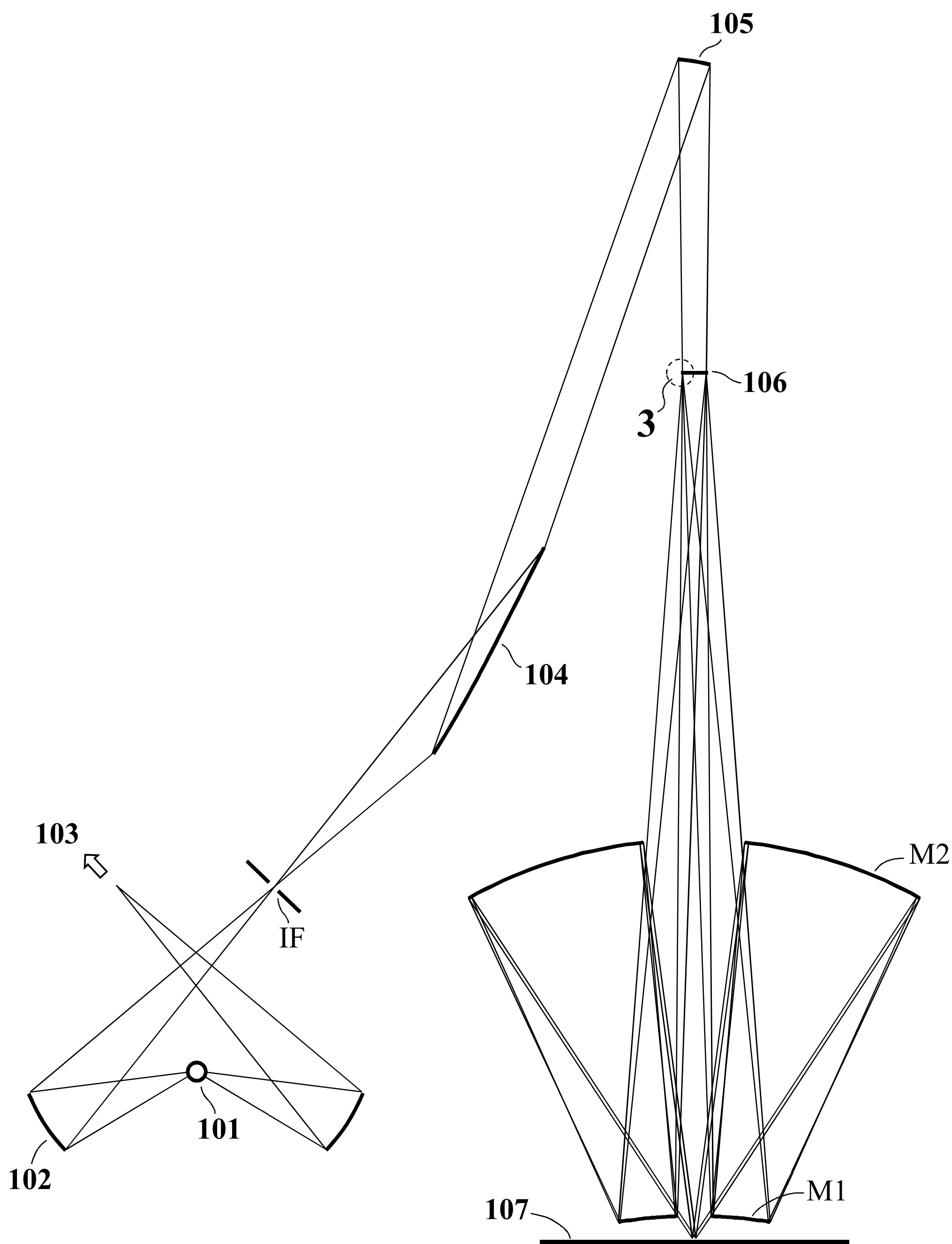

FIG. 1

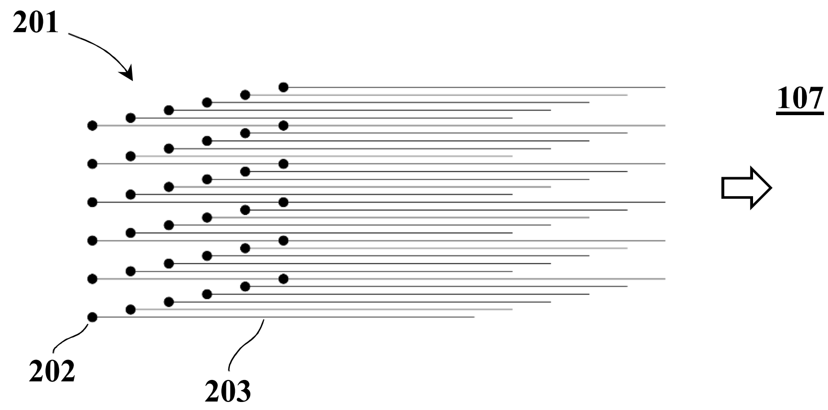

FIG. 2 (Prior Art)

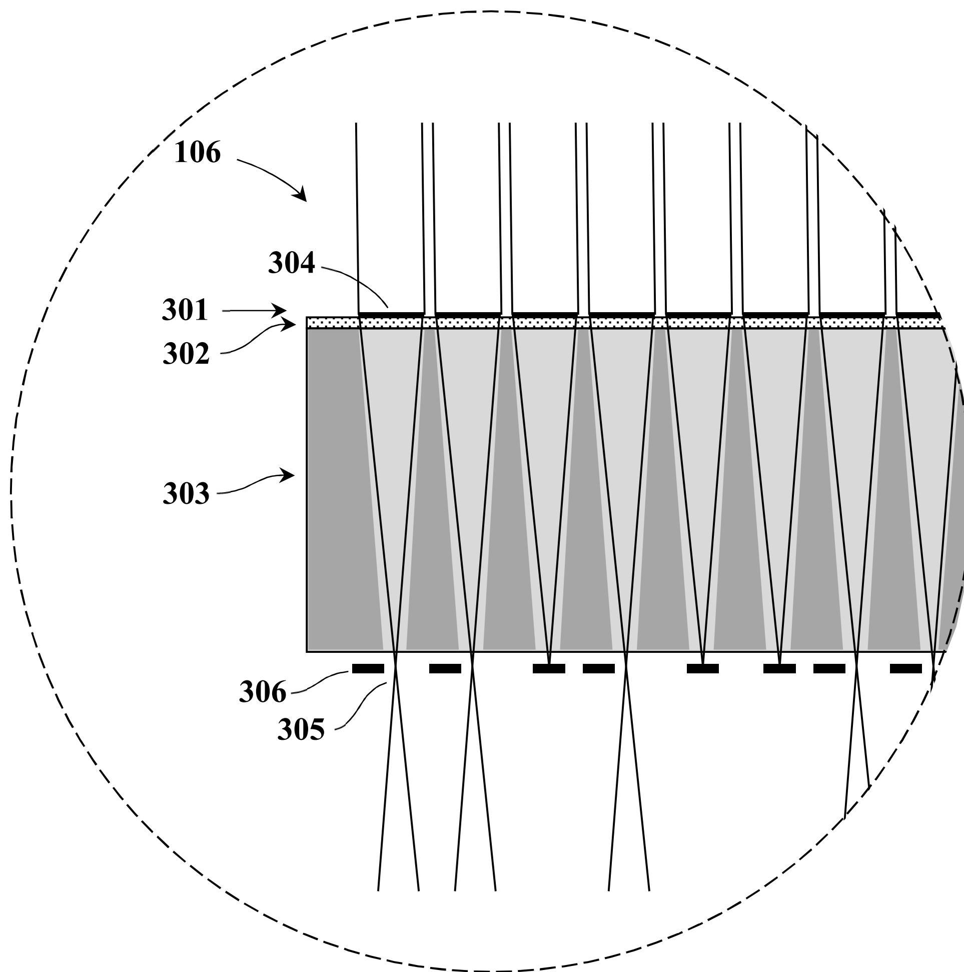

FIG. 3

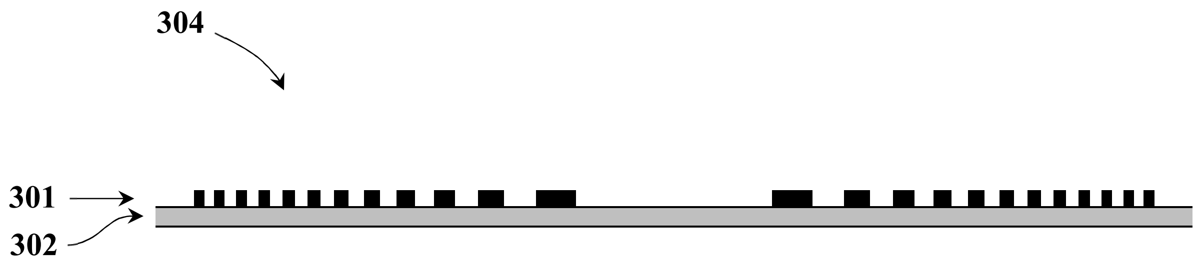

FIG. 4A (Prior Art)

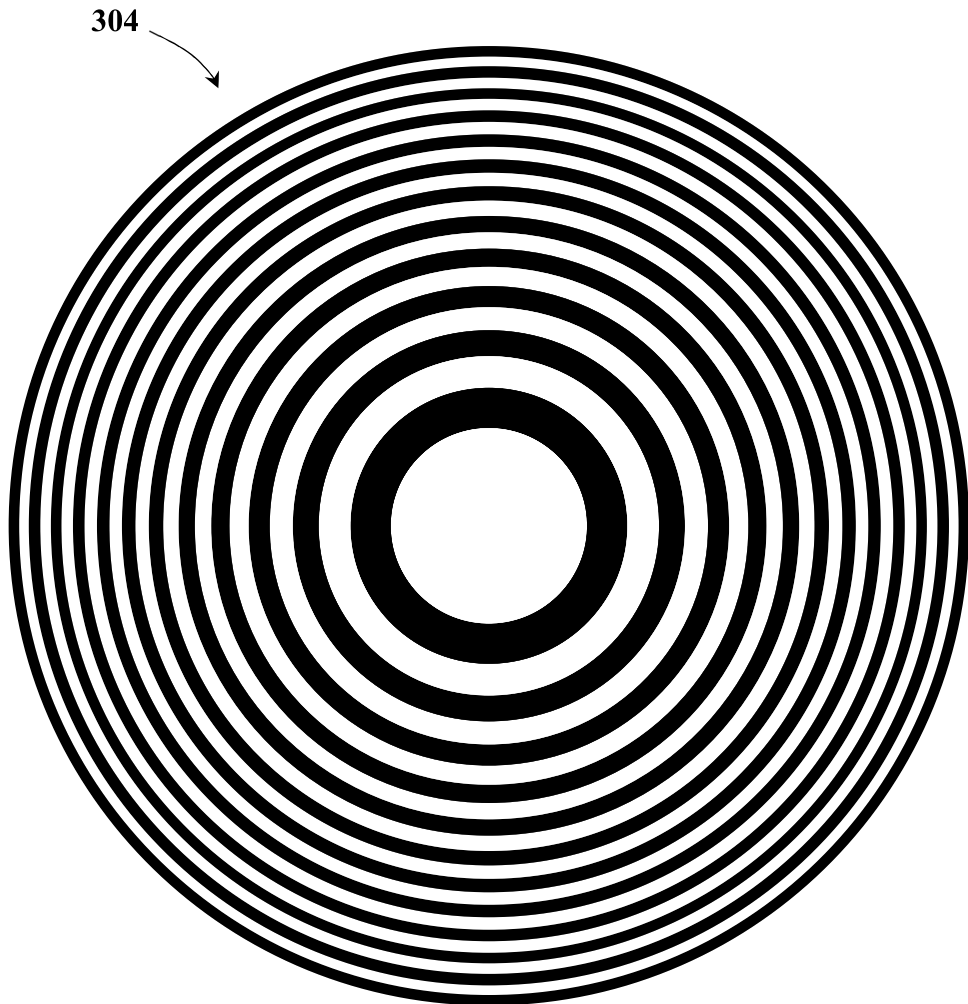

FIG. 4B (Prior Art)

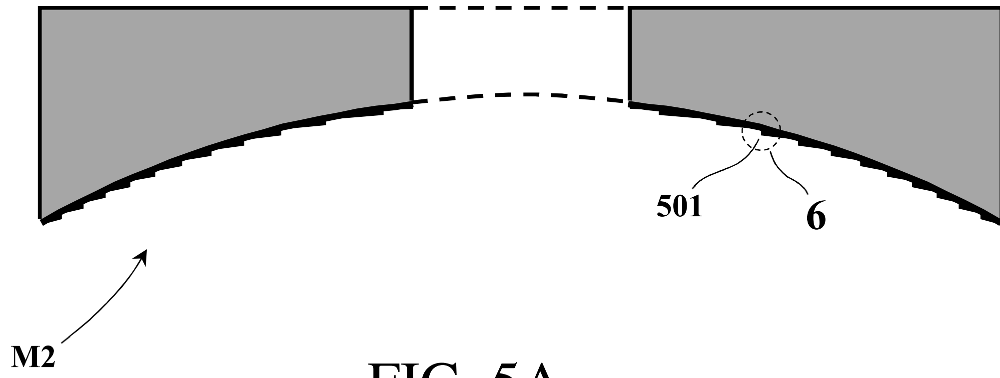

FIG. 5A

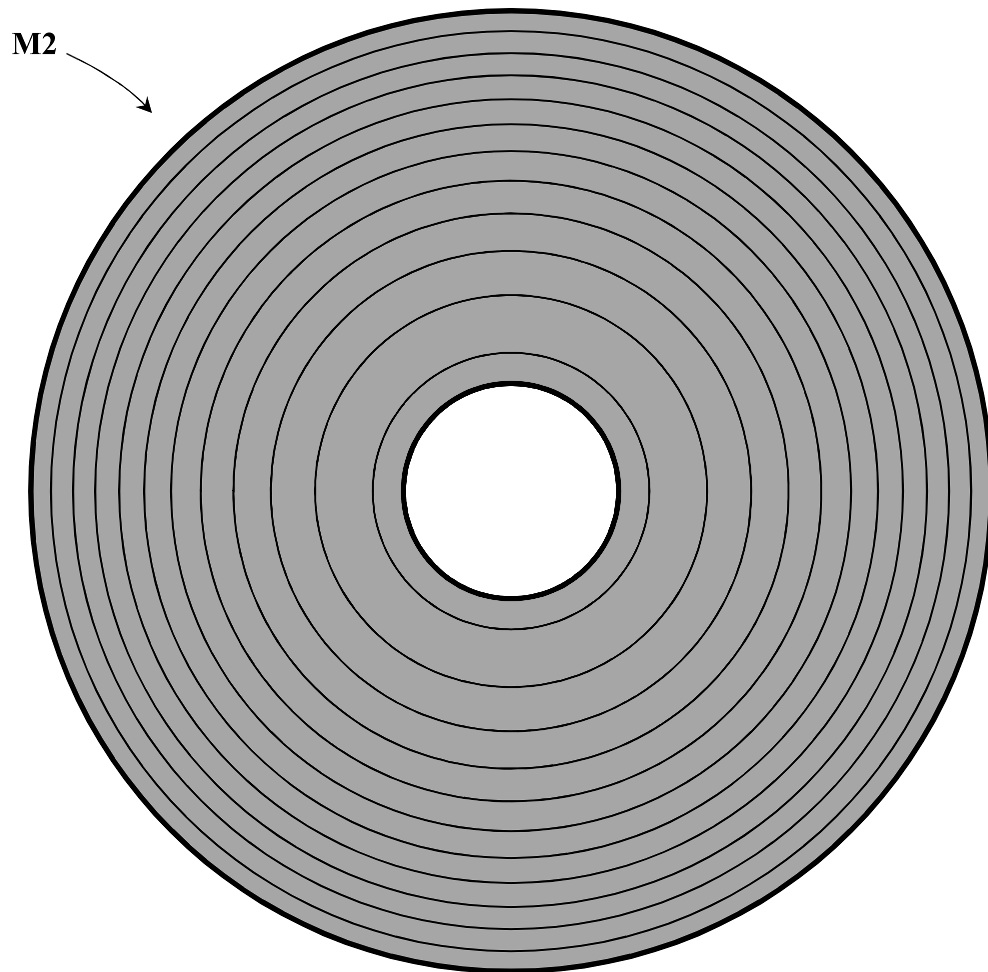

FIG. 5B

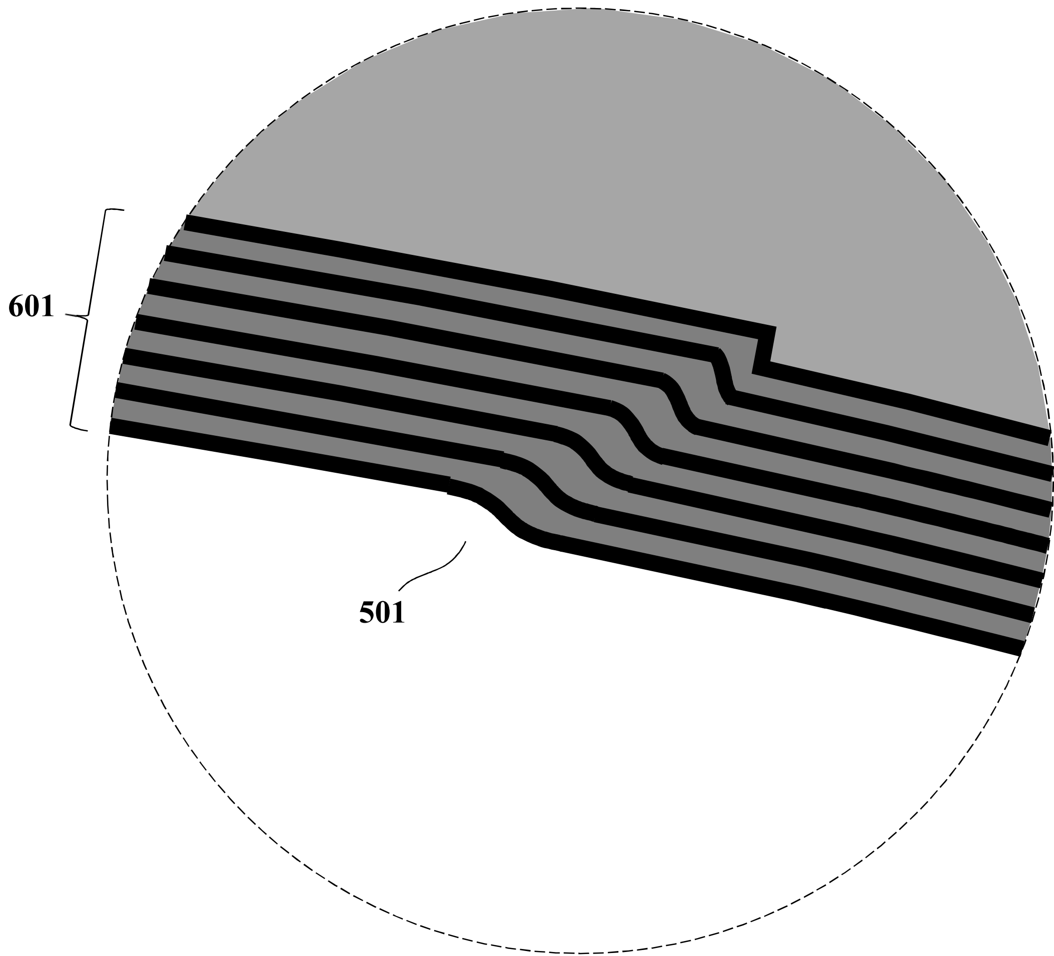

FIG. 6

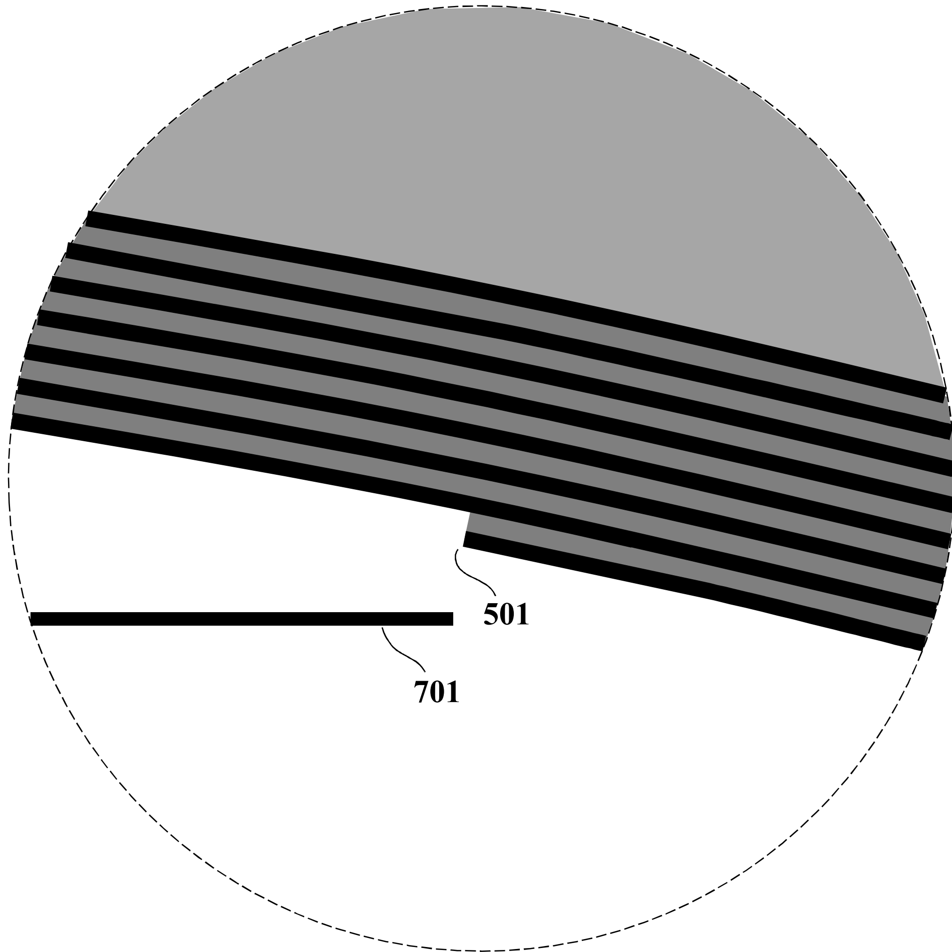

FIG. 7

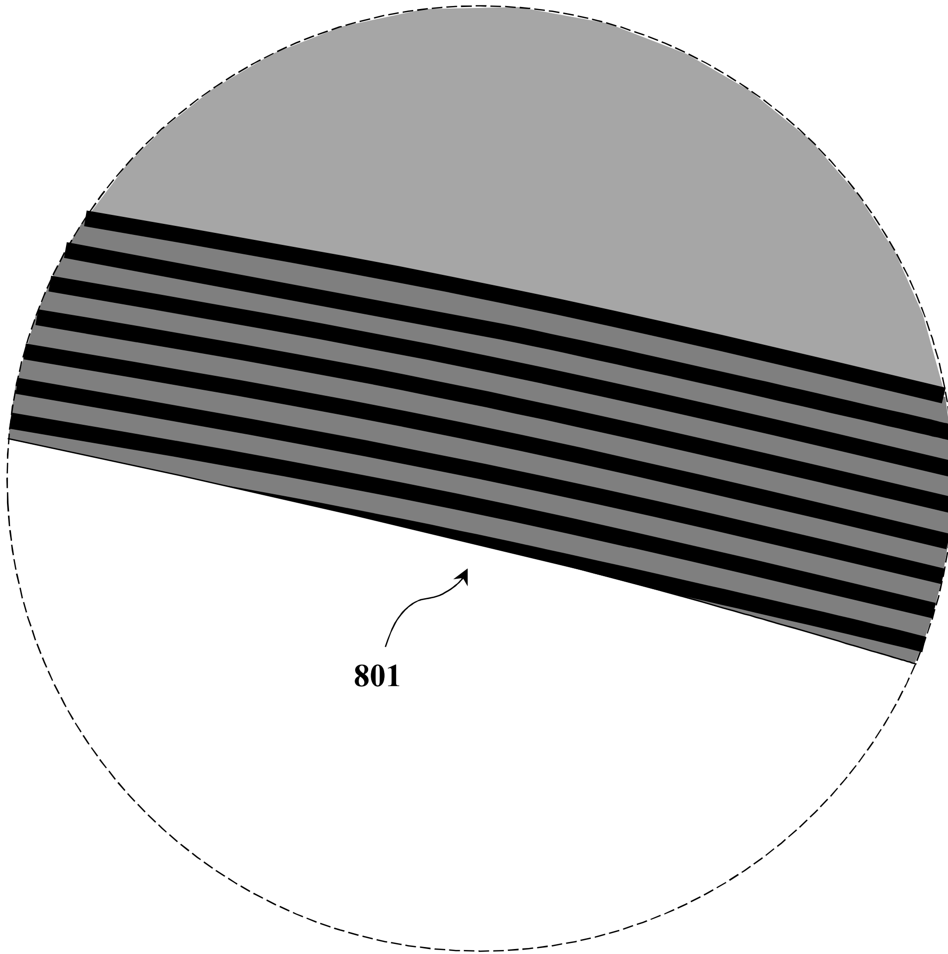

FIG. 8

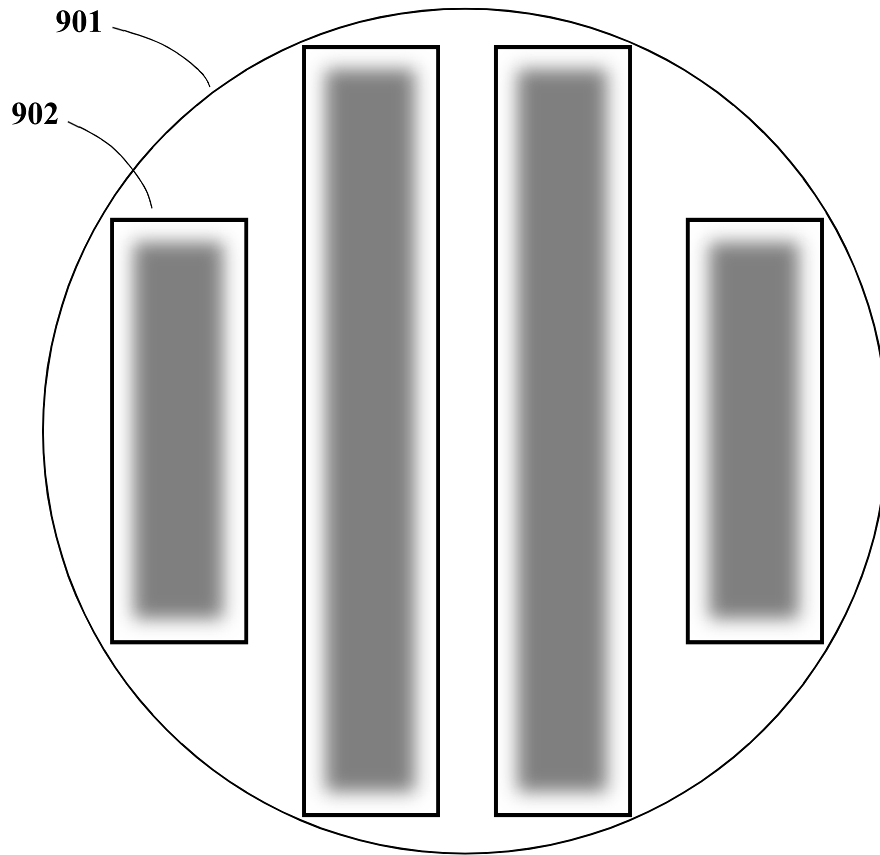

FIG. 9

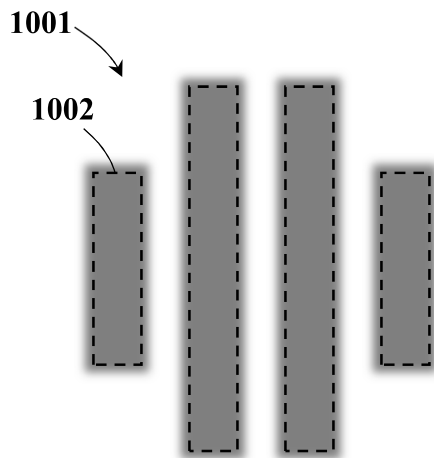

FIG. 10A

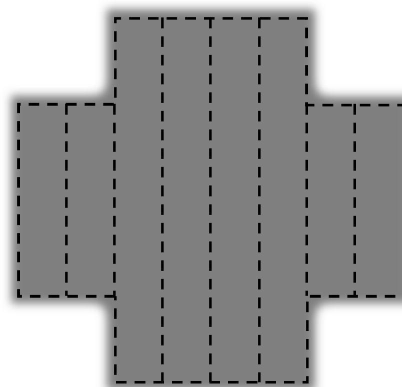

FIG. 10B

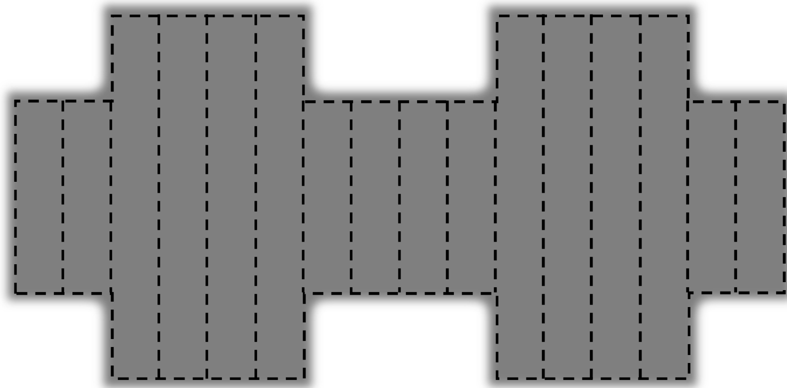

FIG. 10C

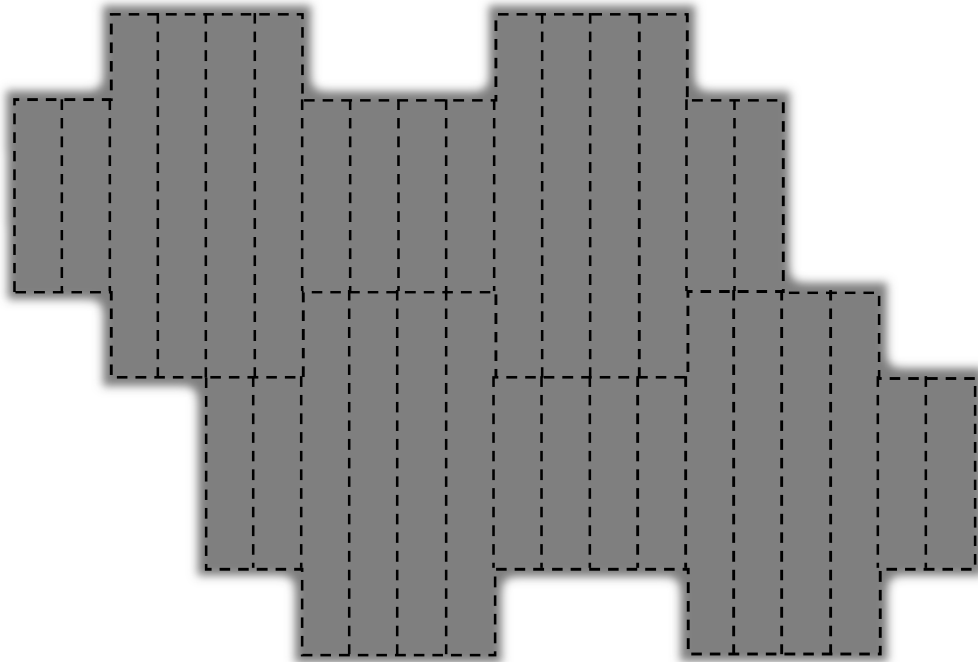

FIG. 10D

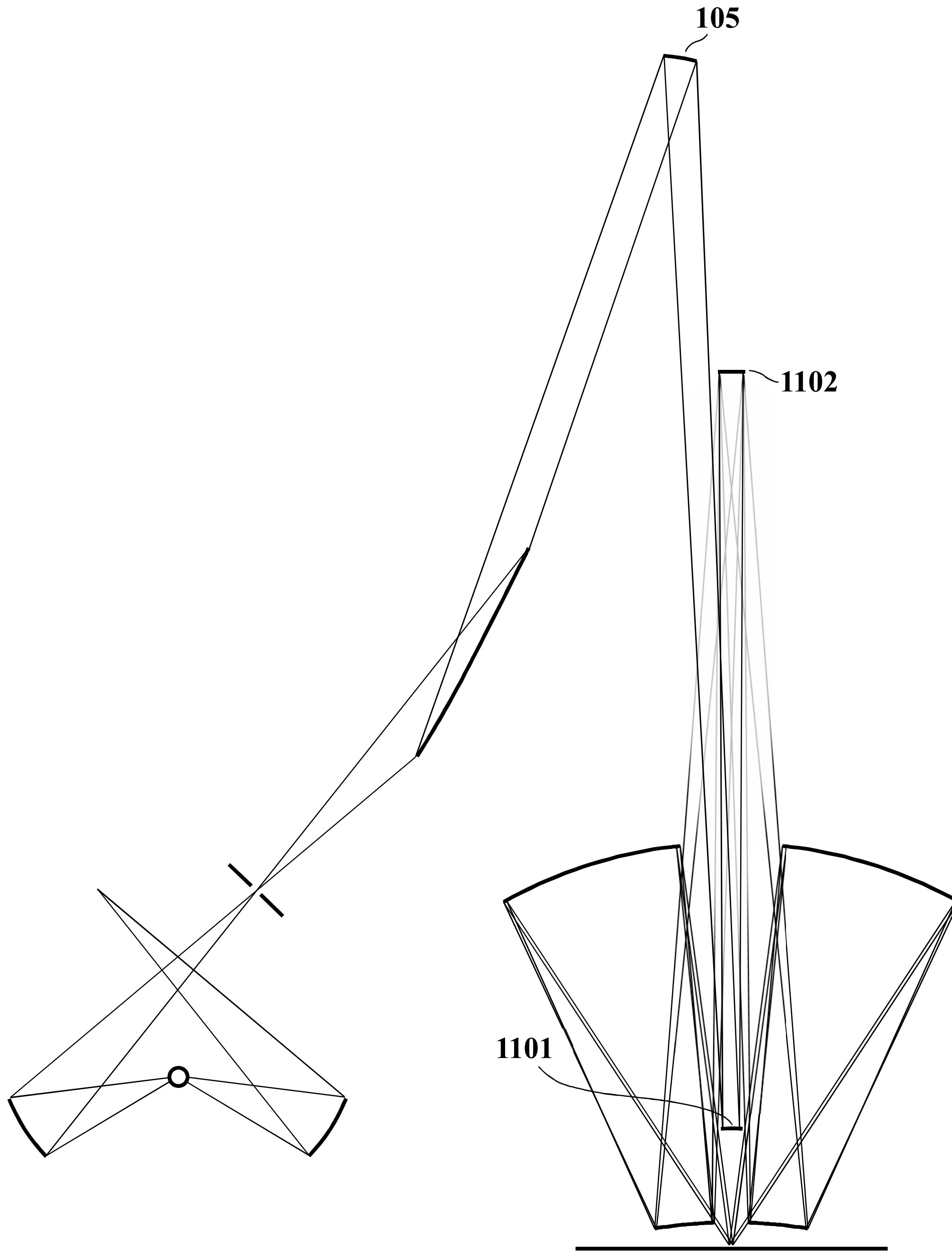

FIG. 11

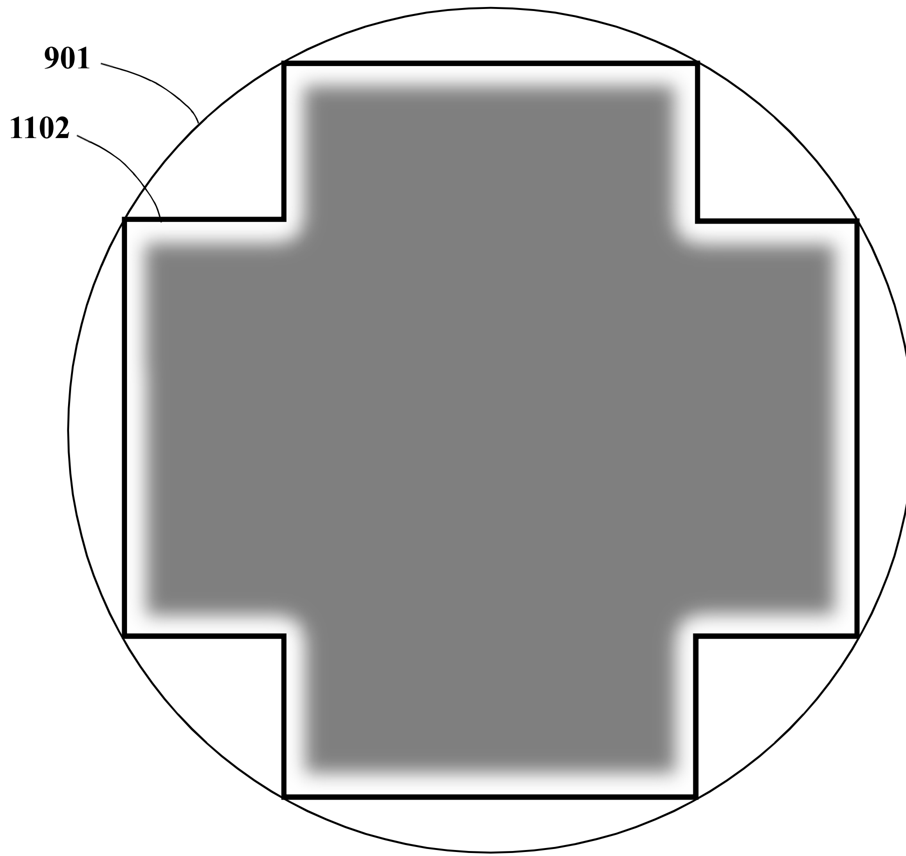

FIG. 12

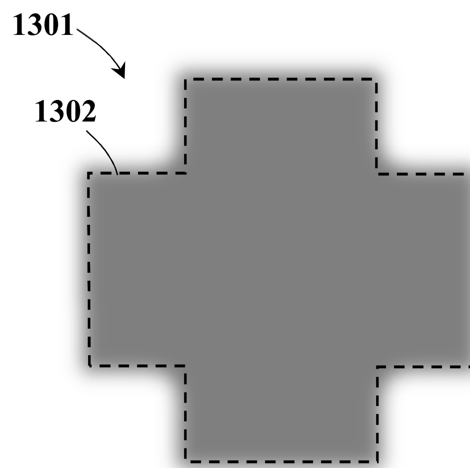

FIG. 13A

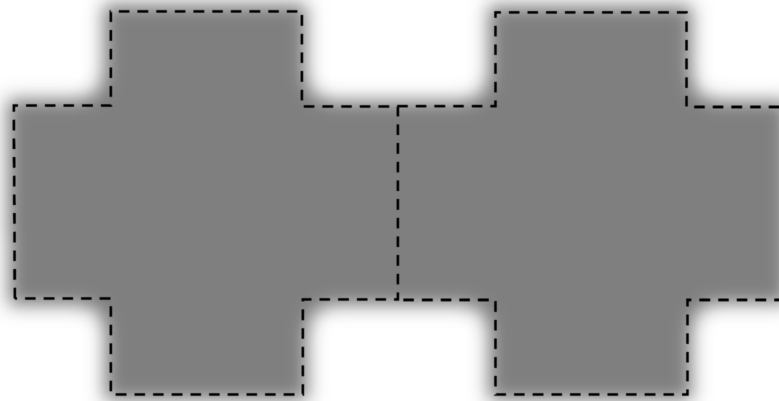

FIG. 13B

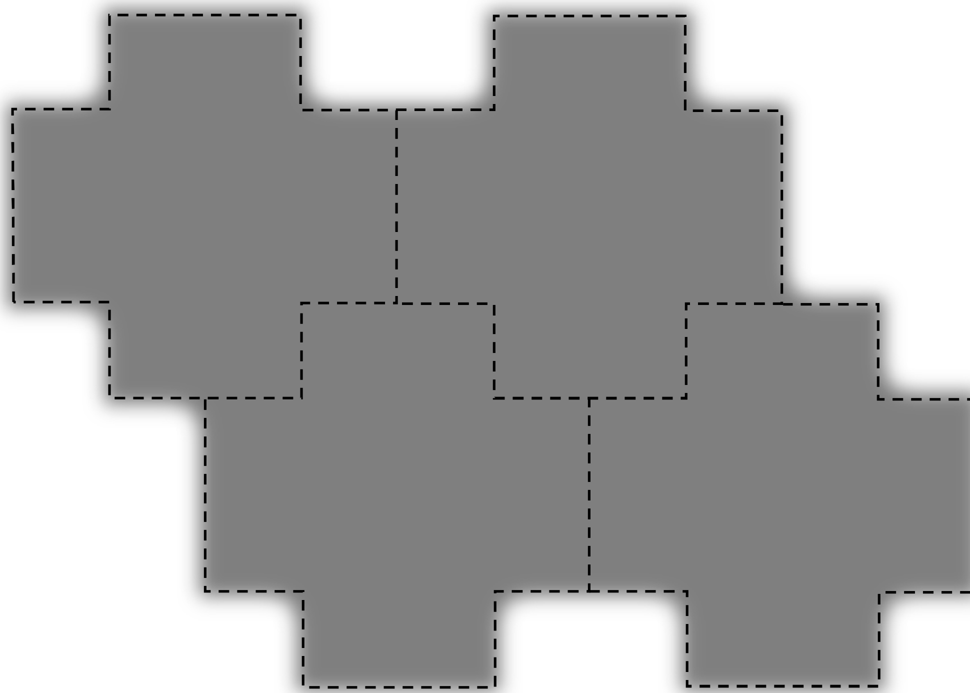

FIG. 13C

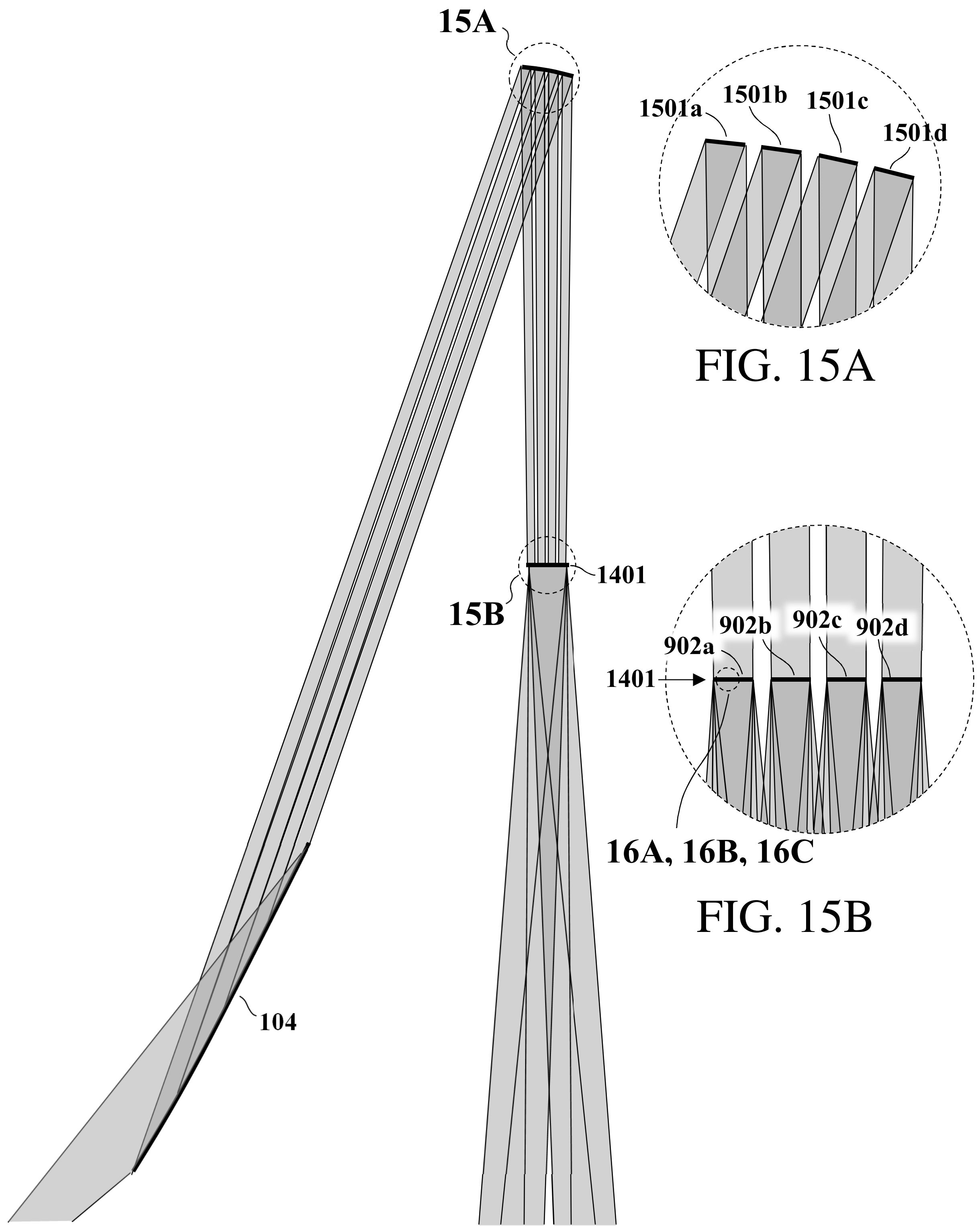

FIG. 15A

FIG. 15B

FIG. 14

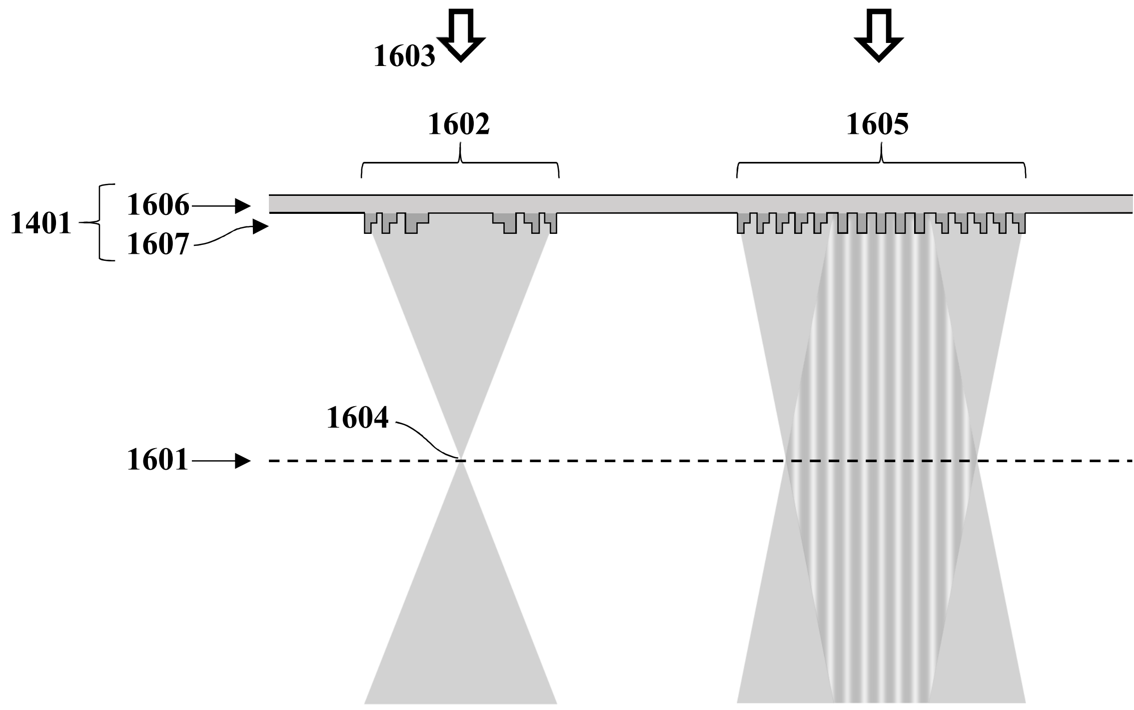

FIG. 16A

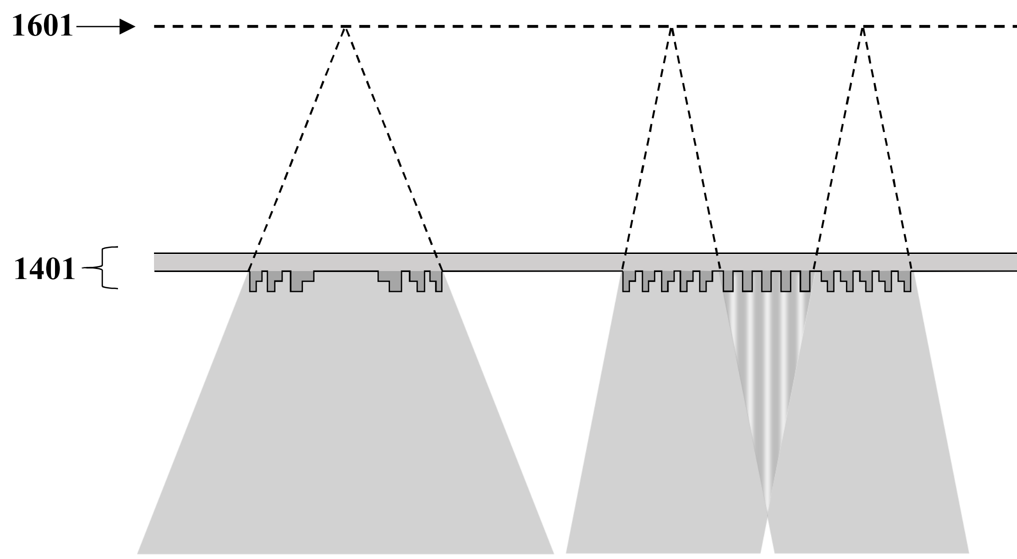

FIG. 16B

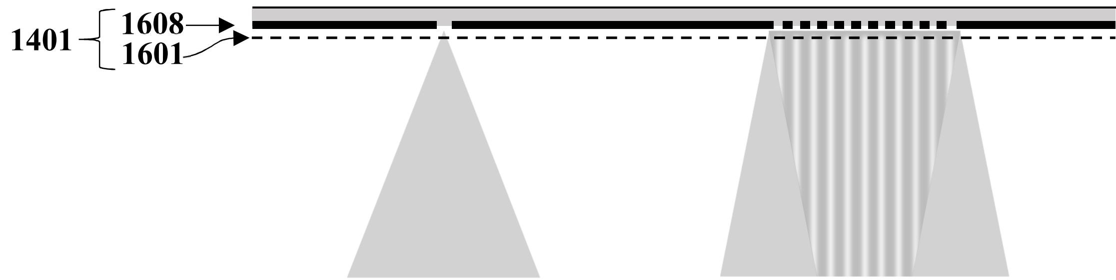

FIG. 16C

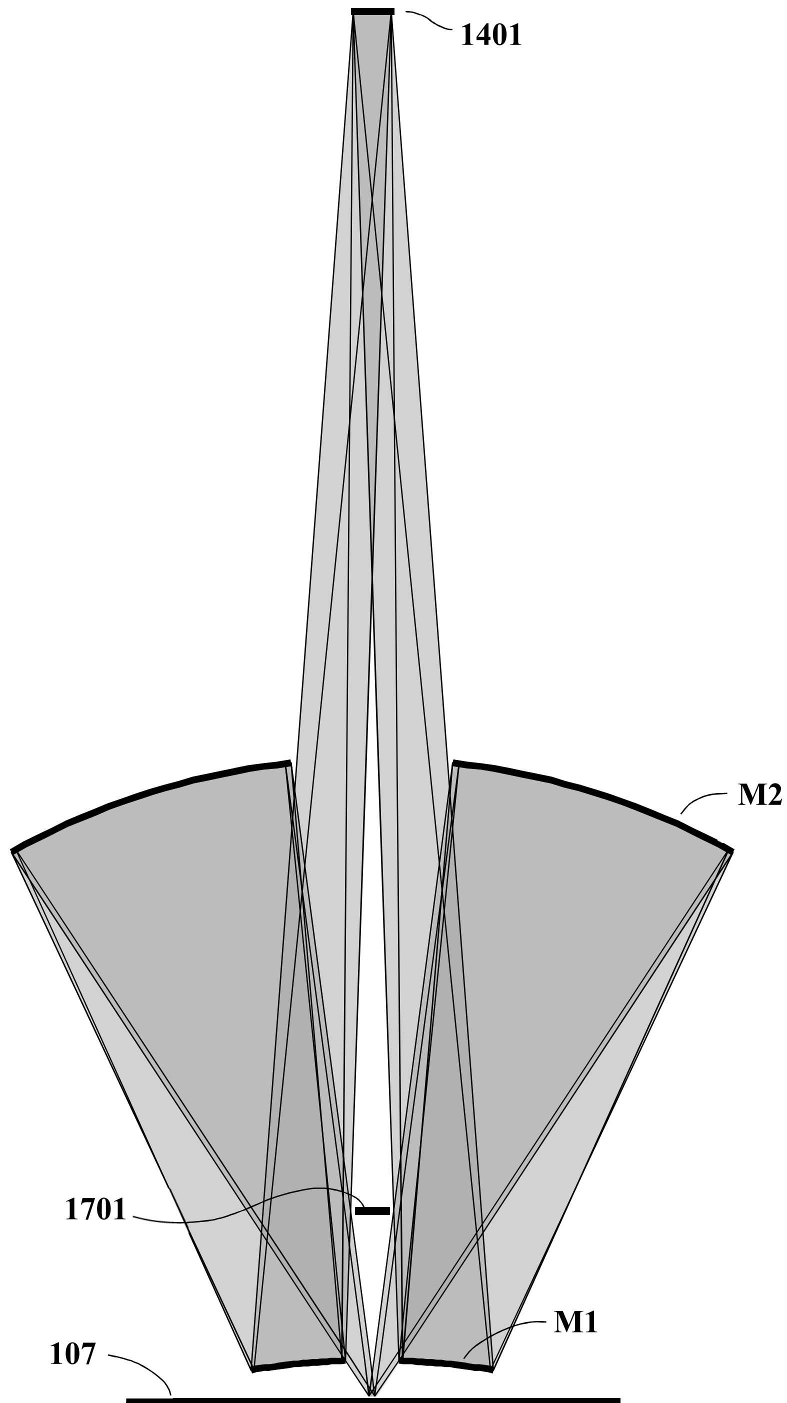

FIG. 17

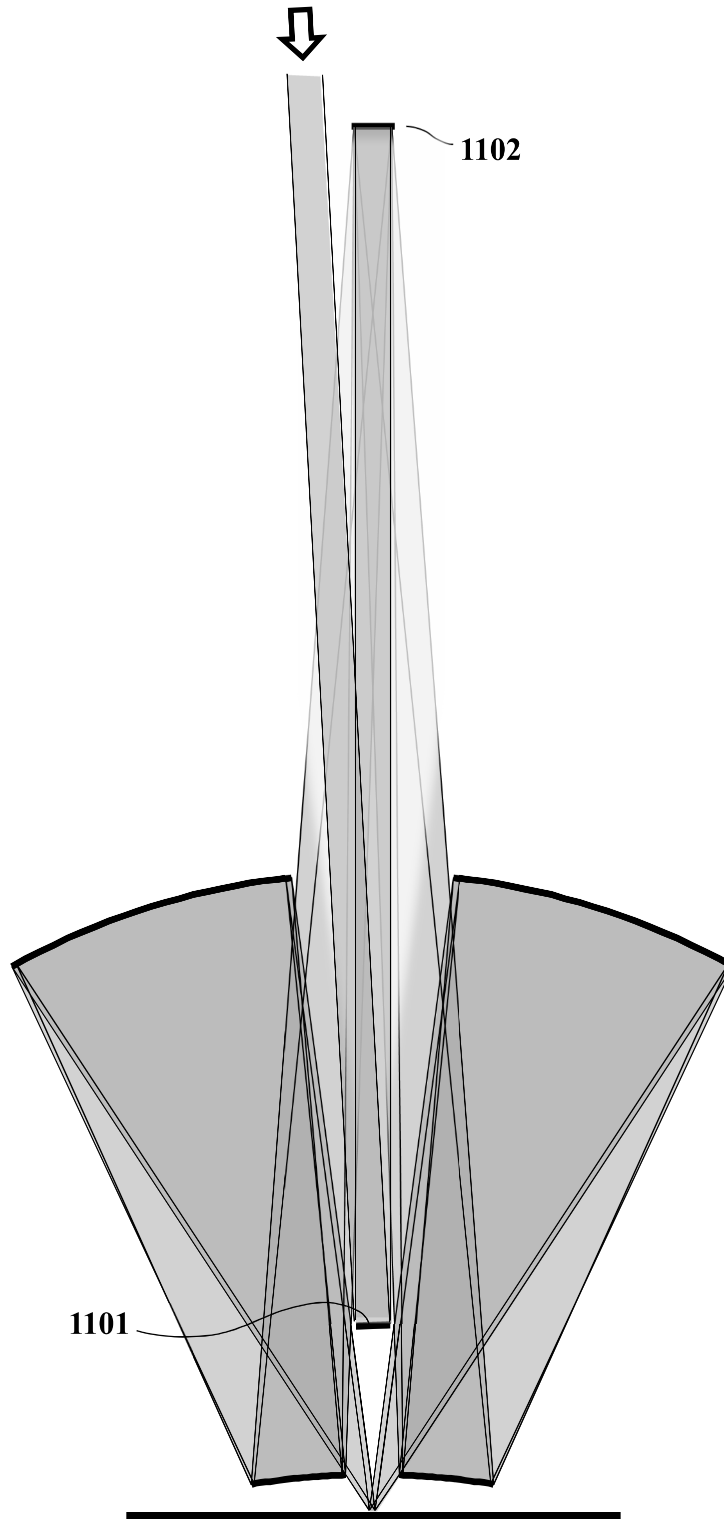

FIG. 18

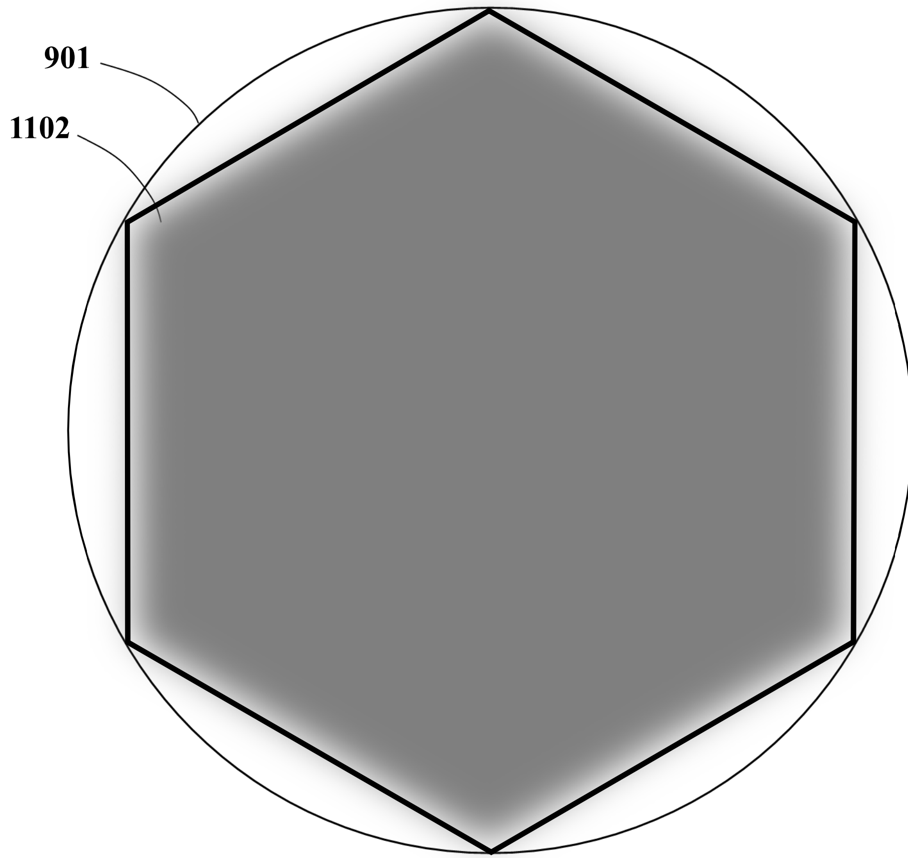

FIG. 19

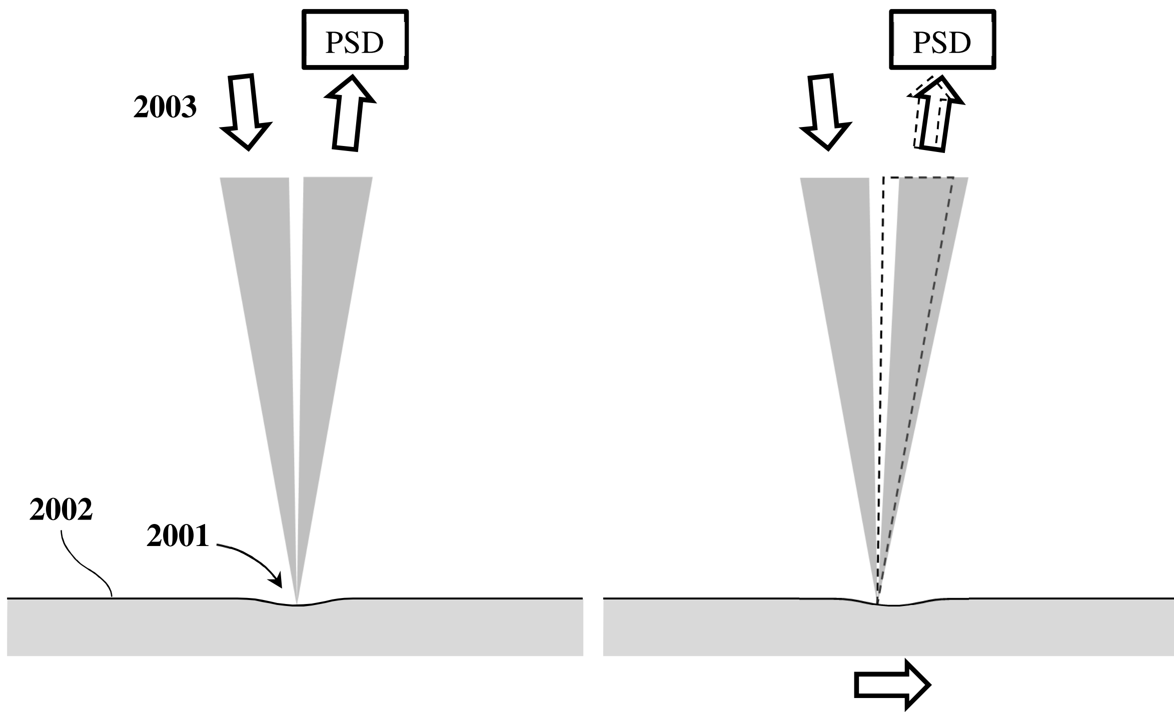

FIG. 20A

FIG. 20B

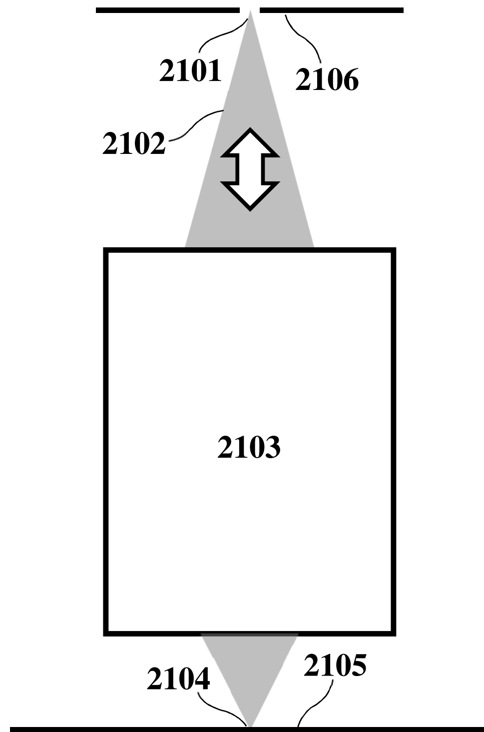

FIG. 21

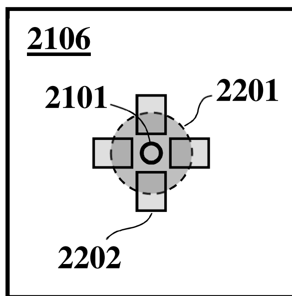

FIG. 22A

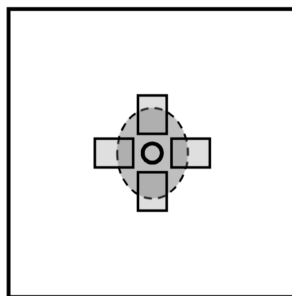

FIG. 22B

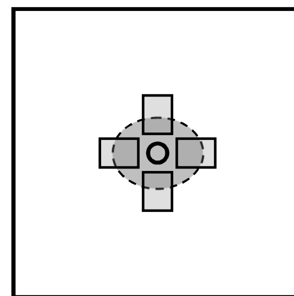

FIG. 22C